Int. J. Heat Mass Transfer. Vol. 33, No. 6, pp. 1247–1261, 1990
Printed in Great Britain

0017–9310/90 $3.00 + 0.00

Analysis of the non-thermal equilibrium condensing flow of a gas through a packed bed

M. SÖZEN and K. VAFAI
Department of Mechanical Engineering, The Ohio State University, Columbus, OH 43210, U.S.A.

(*Received* 12 *April* 1989 *and in final form* 18 *September* 1989)

Abstract—In this paper, the transient forced convective condensing flow of a gas through a packed bed is analyzed. The model developed for this analysis does not employ any local thermal equilibrium assumption between the solid and the fluid phases. Inertial as well as viscous effects are considered in the vapor phase momentum equation by using the Ergun–Forchheimer relation. Thermal charging of the packed bed for two different types of boundary conditions and the condensation in the vapor phase are studied. Qualitative comparisons of the effects of different parameters on condensation reveal that the pressure difference applied across the packed bed, the particle size of the solid phase, and the heat capacity of the solid phase are very influential on condensation. It is observed that although two-dimensional modeling is essential for accurate results in the case of constant wall temperature boundary conditions, one-dimensional modeling would be quite satisfactory in the case of insulated boundary conditions.

1. INTRODUCTION

THE FLOW of a mixture of a vapor and non-condensible gases, such as air and water vapor, through a porous medium, and the accompanying phase change (condensation) in the vapor phase and the multi-phase transport processes involved have received considerable attention through problems related to different applications, such as phase change in building insulation materials [1–3], heat pipe technology [4], and others [5]. The condensing flow of a single vapor phase through a porous medium, on the other hand, has received relatively little attention [6]. A rigorous model which includes the basic thermodynamics of the condensation process and the concept of non-thermal equilibrium between the solid and the fluid phases under the condensing conditions seem to be completely absent. This fact is the main motivation for the present investigation, which is aimed at analyzing the forced convective condensing flow of a vapor through a packed bed. The need for analyzing such problems is a pressing issue in a number of contemporary applications of the packed beds. Packed beds which have been classically used in the chemical industry and for energy storage purposes in the form of pebble bed or rock pile heat storage units, are currently being considered for such applications as a thermal energy storage system for rejection of heat in pulsed space power supplies and some conceptual spacecraft thermal management systems. Moreover, the energy storage effectiveness of the packed beds has been enhanced with the application of encapsulated phase change material, which makes use of the latent heat storage, for the solid particles of the bed [7].

The operating conditions of the packed bed may require gas/vapor flow at high speeds as well as high pressures, which in turn may dictate condensation of the working fluid. This may actually be desirable in order to enhance the amount of thermal energy stored in the packed bed. Therefore, the fundamental study required for analyzing such problems coincides with the aim of the present work.

In this paper, the transient condensing flow of a vapor through a fixed bed of regularly sized spherical solid particles packed in a two-dimensional channel is studied. The vapor considered as the working fluid is Freon-12 (dichlorodifluoromethane or R-12) which is a highly inert and stable compound. It was chosen due to the fact that its critical temperature is well above the temperature ranges considered in this investigation, and because of its relatively high vapor density that enables it to carry more thermal energy per unit volume than the typical gases such as air.

The Ergun–Forchheimer relation is employed as the vapor phase momentum equation in order to account for the inertia effects in addition to the viscous effects. This is very essential for non-Darcy regime flows in porous media. This point has been neglected in many of the previous studies dealing with multi-phase transport phenomena in porous media. Likewise, the previous works on multi-phase transport in porous media almost exclusively employ local thermal equilibrium (LTE) between the solid and fluid phases considered. This assumption may not be satisfactory at all for the step change problems in which, during the early stages of the transport processes there may be considerable difference between the temperatures of the flowing fluid and solid particles. This is also true even during the later stages of the transport processes in high speed flows or high permeability porous media in which the fluid to solid interaction time or surface area respectively may not be large enough to bring the temperatures of the fluid and solid phases close enough for LTE to be a reasonable assumption. The use of such an assumption can, therefore, result in very erratic results especially in the amount of condensation in the vapor phase. The present study makes the necessary provisions for analyzing the difference

NOMENCLATURE

$a_{\sigma\beta}$	specific surface area common to σ and β phases [$m^2\ m^{-3}$]
$a_{\sigma\gamma}$	specific surface area common to σ and γ phases [$m^2\ m^{-3}$]
A	constant in equation (9), 23.4851064
B	constant in equation (9), 2969.2287 [K^{-1}]
c_p	specific heat at constant pressure [$J\ kg^{-1}\ K^{-1}$]
d_p	particle diameter [m]
Da	Darcy number, K/H^2
F	geometric factor defined in equation (10)
g	gravitational acceleration [$m\ s^{-2}$]
G	mass velocity [$kg\ m^{-2}\ s^{-1}$]
$h_{\sigma\beta}$	fluid-to-particle heat transfer coefficient between σ and β phases [$W\ m^{-2}\ K^{-1}$]
$h_{\sigma\gamma}$	fluid-to-particle heat transfer coefficient between σ and γ phases [$W\ m^{-2}\ K^{-1}$]
H	height of the packed bed [m]
k	thermal conductivity [$W\ m^{-1}\ K^{-1}$]
$k_{r\beta}$	relative permeability for fluid phase
$k_{\langle T\rangle}$	coefficient of capillary pressure gradient with respect to temperature [$N\ m^{-2}$]
k_ε	coefficient of capillary pressure with respect to liquid volume fraction [$N\ m^{-2}$]
K	permeability [m^2]
L	length of the packed bed [m]
$\dot{m}$	condensation rate [$kg\ m^{-3}\ s^{-1}$]
P	pressure [$N\ m^{-2}$]
R_γ	gas constant for refrigerant-12 [$J\ kg^{-1}\ K^{-1}$]
Re_p	particle Reynolds number, $\rho_\gamma v^* d_p/\mu_\gamma$
s	saturation, $\varepsilon_\beta/\varepsilon$
S	normalized saturation, $(s-s_{im})/(1-s_{im})$
t	time [s]
T	temperature [K]
u	velocity component in the x-direction [$m\ s^{-1}$]
v	velocity vector [$m\ s^{-1}$].

Greek symbols

ε	porosity
ε_β	volume fraction of liquid phase
ε_γ	volume fraction of vapor phase
ε_σ	volume fraction of solid phase
Δh_{vap}	latent heat of vaporization for refrigerant-12 [$J\ kg^{-1}$]
Θ	dimensionless temperature, $(T-T_0)/(T_{in}-T_0)$
μ	absolute viscosity [$kg\ m^{-1}\ s^{-1}$]
ρ	density [$kg\ m^{-3}$]
$\rho_{\gamma,s}$	saturation vapor density [$kg\ m^{-3}$].

Subscripts

f	fluid (liquid + vapor)
feff	effective property for fluid
in	inlet
0	initial
β	liquid
γ	vapor
σ	solid
σeff	effective property for solid.

Superscripts

f	fluid (liquid + vapor)
β	liquid
γ	vapor
σ	solid
*	reference.

Other symbol

$\langle\ \rangle$	'local volume average' of a quantity.

in the temperatures of the solid and vapor phases by modeling the problem with no LTE assumption.

It should be noted that the authors have reported an investigation on transient, single-phase compressible flow of a vapor/gas through a packed bed [8]. In that study the problem was analyzed by assuming no LTE between the solid and fluid phases, and the inertia effects were accounted for in the fluid phase momentum equation. The conditions under which local thermal equilibrium and/or one-dimensional modeling could be used with reasonable accuracy were thoroughly discussed. In this study, thermal charging of the packed bed for cases with insulated wall and constant wall temperature boundary conditions is analyzed for condensing flow conditions. Qualitative analyses of the effects of different characteristic parameters such as particle Reynolds number, Darcy number and thermophysical properties on the condensation of the vapor phase are also performed.

2. ANALYSIS

Figure 1 depicts the schematic diagram of the problem under consideration. The packed bed is initially filled with the working fluid (Freon-12) at a slightly superheated state and the whole vapor and solid system is at uniform temperature and pressure. R-12 vapor at a higher temperature and pressure from a reservoir is suddenly allowed to flow through the packed bed, thus depositing its thermal energy to the solid particles of the bed. This basically forms a step change in the temperature and pressure at the inlet boundary. In establishing a model for analyzing this problem, the following assumptions and simplifications were employed.

(1) The width of the packed bed is significantly larger than the length and the height, and therefore the problem is essentially two-dimensional.

(2) The vapor phase behaves as an ideal gas.

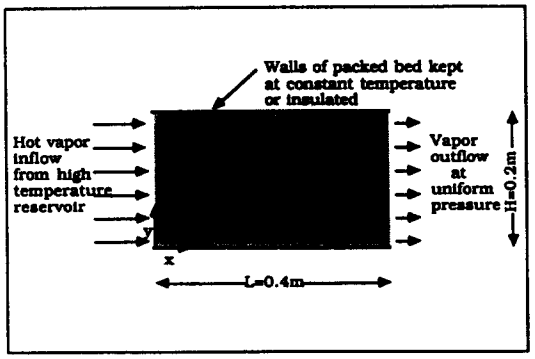

FIG. 1. Schematic diagram of the problem.

(3) There is no local thermal equilibrium (LTE) between the solid and fluid phases but there is LTE between the vapor and liquid phases when there is condensate present in the packed bed.

(4) Natural convection effects are negligible compared to the forced convection in the vapor phase. This essentially yields a one-dimensional flow in the vapor phase.

(5) The solid and liquid phases are incompressible, and the packed bed has uniform porosity and is isotropic.

(6) Boundary and variable porosity effects are neglected.

(7) Inter-particle and intra-particle radiation heat transfer as well as thermal dispersion effects are neglected.

(8) Variations of physical properties such as thermal conductivities, specific heat capacities, viscosity and latent heat of vaporization with temperature are neglected.

2.1. *Governing equations*

The governing conservation equations as well as thermodynamic relations were developed by application of the well-known 'local volume averaging' technique which has been extensively used in developing the models for transport processes in porous media. Considerable information may be obtained with regards to this technique from ref. [9]. The volume-averaged governing equations can be written in the following vectorial forms.

Vapor phase continuity equation

$$\frac{\partial}{\partial t}(\varepsilon_\gamma\langle\rho_\gamma\rangle^\gamma)+\nabla\cdot(\langle\rho_\gamma\rangle^\gamma\langle\mathbf{v}_\gamma\rangle) = -\langle\dot{m}\rangle. \quad (1)$$

Liquid phase continuity equation

$$\frac{\partial\varepsilon_\beta}{\partial t}+\nabla\cdot\langle\mathbf{v}_\beta\rangle-\frac{\langle\dot{m}\rangle}{\rho_\beta}=0. \quad (2)$$

Vapor phase equation of motion

$$\nabla\langle P_\gamma\rangle^\gamma = -\frac{\langle\rho_\gamma\rangle^\gamma F\varepsilon_\gamma}{K_\gamma^{1/2}}[\langle\mathbf{v}_\gamma\rangle\cdot\langle\mathbf{v}_\gamma\rangle]\frac{\langle\mathbf{v}_\gamma\rangle}{|\langle\mathbf{v}_\gamma\rangle|}-\frac{\mu_\gamma}{K_\gamma}\langle\mathbf{v}_\gamma\rangle \quad (3)$$

with assumption (3) above, this equation reduces to

$$\frac{\partial}{\partial x}\langle P_\gamma\rangle^\gamma = -\frac{\langle\rho_\gamma\rangle^\gamma F\varepsilon_\gamma}{K_\gamma^{1/2}}\langle u_\gamma\rangle^2-\frac{\mu_\gamma}{K_\gamma}\langle u_\gamma\rangle. \quad (3a)$$

Liquid phase equation of motion

$$\langle\mathbf{v}_\beta\rangle = -\frac{k_{r\beta}K}{\mu_\beta}\{k_\varepsilon\nabla\beta+k_{\langle T\rangle}\nabla\langle T_f\rangle^f+(\rho_\beta-\langle\rho_\gamma\rangle^\gamma)\mathbf{g}\}. \quad (4)$$

Fluid phase energy equation

$$[\varepsilon_\beta\rho_\beta(c_p)_\beta+\varepsilon_\gamma\langle\rho_\gamma\rangle^\gamma(c_p)_\gamma]\frac{\partial\langle T_f\rangle^f}{\partial t}-\langle\dot{m}\rangle\Delta h_{vap}$$
$$+[\rho_\beta(c_p)_\beta\langle\mathbf{v}_\beta\rangle+\langle\rho_\gamma\rangle^\gamma(c_p)_\gamma\langle\mathbf{v}_\gamma\rangle]$$
$$\cdot\nabla\langle T_f\rangle^f = \nabla\cdot[k_{feff}\nabla\langle T_f\rangle^f]$$
$$+h_{\sigma\beta}a_{\sigma\beta}[\langle T_\sigma\rangle^\sigma-\langle T_f\rangle^f]+h_{\sigma\gamma}a_{\sigma\gamma}[\langle T_\sigma\rangle^\sigma-\langle T_f\rangle^f]. \quad (5)$$

Solid phase energy equation

$$\varepsilon_\sigma\rho_\sigma(c_p)_\sigma\frac{\partial\langle T_\sigma\rangle^\sigma}{\partial t} = \nabla\cdot[k_{\sigma eff}\nabla\langle T_\sigma\rangle^\sigma]-h_{\sigma\beta}a_{\sigma\beta}$$
$$\times[\langle T_\sigma\rangle^\sigma-\langle T_f\rangle^f]-h_{\sigma\gamma}a_{\sigma\gamma}[\langle T_\sigma\rangle^\sigma-\langle T_f\rangle^f]. \quad (6)$$

Volume constraint relation

$$\varepsilon_\sigma+\varepsilon_\gamma(t)+\varepsilon_\beta(t)=1. \quad (7)$$

Equation of state for vapor phase

$$\langle P_\gamma\rangle^\gamma = \langle\rho_\gamma\rangle^\gamma R_\gamma\langle T_f\rangle^f. \quad (8)$$

Thermodynamic relation for the saturation density of vapor

$$\rho_{\gamma,s} = \frac{\exp\left(A-\frac{B}{T_f}\right)}{R_\gamma T_f} \quad (9)$$

where A and B are constants, T_f is in Kelvin and $\rho_{\gamma,s}$ is in kg m^{-3}. These yield nine equations in nine unknowns, namely $\varepsilon_\beta(t)$, $\varepsilon_\gamma(t)$, $\langle\rho_\gamma\rangle^\gamma$, $\langle\mathbf{v}_\gamma\rangle$, $\langle\mathbf{v}_\beta\rangle$, $\langle P_\gamma\rangle^\gamma$, $\langle T_f\rangle^f$, $\langle T_\sigma\rangle^\sigma$, $\langle\dot{m}\rangle$.

The effective thermal conductivities were modeled in the form

$$k_{\sigma eff} = \varepsilon_\sigma k_\sigma$$
$$k_{feff} = \varepsilon_\gamma k_\gamma+\varepsilon_\beta k_\beta. \quad (10)$$

The permeability of the packed bed of spherical particles is given in the following form [10]:

$$K = \frac{\varepsilon^3 d_p^2}{150(1-\varepsilon)^2} \quad (11)$$

where ε is the porosity and d_p the particle diameter. The permeability of the vapor phase, K_γ, and the geometric factor, F, in the vapor phase momentum equation can be expressed as functions of d_p and ε_γ as [10, 11]

$$K_\gamma = \frac{\varepsilon_\gamma^3 d_p^2}{150(1-\varepsilon_\gamma)^2}$$

$$F = \frac{1.75}{\sqrt{(150)\varepsilon_\gamma^{3/2}}}. \quad (12)$$

The relative permeability of the liquid phase follows from the one suggested in ref. [12] as

$$k_{r\beta} = S^3$$

where

$$S = \frac{s - s_{im}}{1 - s_{im}}$$

and

$$s = \frac{\varepsilon_\beta}{\varepsilon} = \frac{\varepsilon_\beta}{1-\varepsilon_\sigma} \quad (13)$$

where S is the normalized saturation, s the absolute saturation and s_{im} the 'immobile' saturation. The value of 0.1 used for s_{im} in ref. [13] will be used in the present work because of the lack of any better experimental finding. With this value of s_{im}, the critical value of ε_β at which liquid phase becomes mobile was found to be 0.039, with the value of porosity of the packed bed taken to be 0.39, which is the average asymptotic value for packed beds in which the particle diameter to packed bed diameter is below a certain value [14]. For all the cases studied in the present investigation the maximum value of ε_β never reached $\varepsilon_{\beta crit}$ and therefore the liquid was always immobile (in the pendular state). It should be noted that the liquid was not assumed to be immobile in the modeling of the problem, but the fact that it turned out to be immobile was the consequence of the governing physical conditions of the problem.

The fluid-to-solid heat transfer coefficients were based on the empirical correlations established in previously performed experimental studies. The empirical correlations established in ref. [15] were found to be suitable for use for the ranges of particle Reynolds numbers (Re_p) that were considered in the present work. The experimental results which were originally expressed for the Colburn–Chilton j_h-factor were manipulated to yield the following forms for the fluid-to-solid heat transfer coefficient:

$$h_{\sigma j} = 1.064(c_p)_j G_j \left[\frac{c_p \mu}{k}\right]_j^{-2/3} \left[\frac{d_p G}{\mu}\right]_j^{-0.41} \quad \text{for} \quad \frac{d_p G}{\mu} \geqslant 350$$

$$h_{\sigma j} = 18.1(c_p)_j G_j \left[\frac{c_p \mu}{k}\right]_j^{-2/3} \left[\frac{d_p G}{\mu}\right]_j^{-1} \quad \text{for} \quad \frac{d_p G}{\mu} \leqslant 450 \quad (14)$$

where G represents the mass flow rate through a unit surface area perpendicular to the direction of flow and the subscript j denotes β or γ for the liquid or vapor phase, respectively.

The specific surface area of the packed bed for the vapor phase may be expressed in the following form:

$$a_{\sigma\gamma} = \frac{6(1-\varepsilon_\gamma - \varepsilon_\beta)}{d_p}. \quad (15)$$

Strictly speaking, this correlation was derived from geometric considerations for a fully saturated packed bed of spherical particles for a single fluid phase, in the form $a = 6(1-\varepsilon)/d_p$ in ref. [16]. However, since ε_β is very small (<0.01) compared to ε_γ (approximately 0.38–0.39) equation (15) provides a very good estimate for $a_{\sigma\gamma}$. Also, due to the fact that the liquid phase is always immobile, $h_{\sigma\beta}$ is zero for all the cases considered and therefore there is no need for estimating $a_{\sigma\beta}$, although this estimation may be simply carried out based on a liquid-to-vapor volume fraction.

2.2. *Boundary and initial conditions*

The problem considered in the present investigation deals with a packed bed which is initially filled with R-12 which is at uniform temperature and pressure and in thermal equilibrium with the solid particles. The initial conditions, therefore, take the following mathematical form:

$$T_f(x,y,t=0) = T_0$$
$$T_\sigma(x,y,t=0) = T_0$$
$$P_\gamma(x,y,t=0) = P_0. \quad (16)$$

The pressure on the right boundary is kept at a value equal to the initial pressure in the packed bed while vapor at a fixed high temperature and pressure is supplied at the left boundary. The mathematical form of the left and right boundary conditions may be expressed as

$$T_f(x=0,y,t) = T_{in}$$
$$P_\gamma(x=0,y,t) = P_{in} \quad \text{at} \quad t > 0^+.$$
$$P_\gamma(x=L,y,t) = P_{out} = P_0 \quad (17)$$

Also, when insulated boundary conditions are used at the top and bottom boundaries, we have

$$k_{eff}\left.\frac{\partial T}{\partial y}\right|_{y=0,\,y=H} = 0 \quad \text{for both } T_f \text{ and } T_\sigma \quad (18)$$

and when constant temperature boundary conditions are used at the top and bottom walls, the boundary conditions can be expressed as

$$T_f(x,y=0,t) = T_\sigma(x,y=0,t) = T_{bot} = T_0$$
$$T_f(x,y=H,t) = T_\sigma(x,y=H,t) = T_{top} = T_0. \quad (19)$$

The numerical values of different parameters used as initial and boundary conditions are given as follows:

$$T_0 = 300\ \text{K}, \quad P_0 = 796\ \text{kPa},$$

$$T_{in} = 350\ \text{K}, \quad P_{out} = 796\ \text{kPa}$$

and the value of P_{in} was different for different cases ranging between 800 and 866 kPa. The numerical values of the other physical data used in computations are as follows:

$$k_\gamma = 0.0097\,\text{W m}^{-1}\text{K}^{-1}, \quad (c_p)_\gamma = 710\,\text{J kg}^{-1}\text{K}^{-1},$$
$$\mu_\gamma = 12.6\times10^{-6}\,\text{kg m}^{-1}\text{s}^{-1},$$
$$R_\gamma = 0.0687588\,\text{J kg}^{-1}\text{K}^{-1},$$
$$\Delta h_{vap} = 111.3\times10^{3}\,\text{J kg}^{-1}, \quad k_\beta = 0.0545\,\text{W m}^{-1}\text{K}^{-1},$$
$$(c_p)_\beta = 1115\,\text{J kg}^{-1}\text{K}^{-1},$$
$$\mu_\beta = 179.2\times10^{-6}\,\text{kg m}^{-1}\text{s}^{-1},$$
$$\rho_\beta = 1190.35\,\text{kg m}^{-3},$$
$$k_\sigma = 35\,\text{W m}^{-1}\text{K}^{-1}, \quad \rho_\sigma = 11\,340\,\text{kg m}^{-3},$$
$$(c_p)_\sigma = 129\,\text{J kg}^{-1}\text{K}^{-1} \quad \text{(for lead)}$$
$$k_\sigma = 43\,\text{W m}^{-1}\text{K}^{-1}, \quad \rho_\sigma = 7800\,\text{kg m}^{-3},$$
$$(c_p)_\sigma = 473\,\text{J kg}^{-1}\text{K}^{-1} \quad \text{(for steel)}.$$

2.3. *Solution*

The governing equations for the problem under consideration are coupled, making analytical solution impossible. For this reason it was necessary to utilize numerical solution techniques, namely the finite difference method. Due to the nature of the governing equations, the more appropriate explicit schemes were utilized. Forward differencing was used in the temporal derivative terms whereas central differencing was used for the spatial derivatives except for the convective terms for which upwind differencing was employed. The spatial derivatives on the left and right as well as top and bottom boundaries were formed by forward or backward differencing whichever appropriate.

Depending on whether phase change (condensation) takes place in the vapor phase or not, the set of unknown variables and governing equations change. The vapor phase continuity equation plays an important role in determining the solution format of the governing equations. It should be emphasized here that the basic criterion which governs the phase change (condensation) is the attainment of the saturation density. At any point where the vapor density reaches the saturation density, at that point condensation will occur.

The stability of the numerical scheme was insured by choosing a proper combination of Δx, Δy and Δt. A systematic decrease in the grid size was used to obtain the convergence of the numerical scheme, and the corresponding stable Δt was employed. A compromise, however, had to be made between the accuracy and the computer CPU time required for the computational runs. A 41×21 grid configuration (which gives a dimensionless Δx of 0.025) was found to yield qualitatively and quantitatively good results for the condensation period and very good results for the later stages of the problem. It was found that the results obtained by using the 41×21 mesh did not differ more than 2% from the results obtained by using an 81×41 mesh. The largest difference was in the results related to the computation of the condensation rates and total condensate accumulation both of which involved integration over the associated grid volume. This volume was in turn dependent on the grid spacing. Since the CPU time for these runs becomes excessive even on a CRAY XMP/28, the accuracy obtained by using a 41×21 mesh was deemed to be sufficient.

3. RESULTS AND DISCUSSION

As mentioned earlier, the analysis of the transient forced convective condensing flow of a single vapor through a packed bed, for a non-thermal equilibrium case and in which inertia effects are considered, has not been modeled and solved rigorously in the way it is done in the present investigation. Consequently the solution of the different field variables undertaken here has not been carried out before. Therefore, there is no suitable reference in the literature for comparing the results of this study for all the field variables involved. It is, however, possible to benchmark the results of the computer program which was developed, against the most pertinent analytical solutions for different aspects of the transport phenomena in porous media, which are limiting cases for the current problem.

This benchmarking was performed in two main parts for the limiting case of no phase change in the vapor phase. The first part dealt with the energy transfer in an incompressible fluid flow through a porous medium in which there is no local thermal equilibrium between the solid and the fluid phases. The second part dealt with the momentum transport (pressure and velocity distribution) in an isothermal flow of an ideal gas through a porous medium. These were the most relevant sources, with field variables translatable to those of the present work, that could be located. For benchmarking the energy transport, our numerical results were compared against the analytical solution of the Schumann model which was presented in ref. [17]. Figure 2 depicts this comparison for the solid and fluid phase temperature distributions in terms of the dimensionless variables used in ref. [17]. The figure shows excellent agreement between the analytical and numerical solutions. Benchmarking of the momentum transport was carried out against the analytical solution of a one-dimensional isothermal flow of an ideal gas through a semi-infinite porous medium that has been obtained in ref. [18] by the use of perturbation methods. Although this analytical solution was for a semi-infinite porous medium, comparison of the results of the numerical code was safely performed for small times during which the pressure propagation in the packed bed takes place only up to the exit of the bed. Figure 3 shows the comparison of the analytical solution with the solution of the present numerical

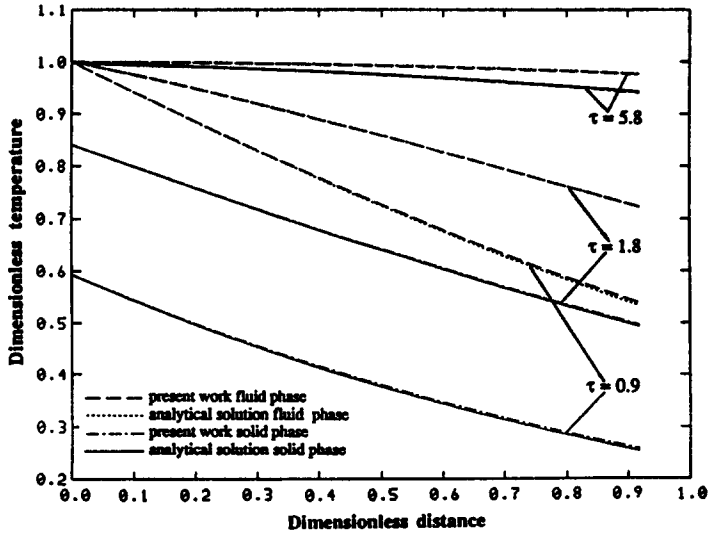

FIG. 2. Comparison of the numerical results with the analytical results in ref. [17].

scheme in terms of the dimensionless pressure as it appears in ref. [18]. As may be seen from this figure, the agreement between the two solutions is very good.

The results that will be presented for the computational runs performed, will be in terms of non-dimensionalized variables. Variables $\langle P_\gamma \rangle^\gamma$, $\langle \rho_\gamma \rangle^\gamma$, and $\langle \mathbf{v}_\gamma \rangle$ are non-dimensionalized by using the corresponding reference quantities, namely P^*, ρ^*, and v^*. P^* was chosen to be 100 kPa, ρ^* was calculated from the equation of state by using P^* and the initial temperature T_0. The reference velocity, v^*, was computed from the vapor phase momentum equation using a pressure gradient which was based on the global pressure difference applied across the packed bed and a density which was calculated from the equation of state by using T_0 and P_{av} (the average of the inlet and exit pressures). Temperatures of the solid and fluid phases are nondimensionalized in the form $\Theta = (T-T_0)/(T_{in}-T_0)$. Time, t, is kept in dimensional form for giving an insight of the actual magnitudes of the durations involved. The same thing is done for the condensation rate data and the total condensate variations as well as for the thermal charging data of the packed bed.

Two distinctly noticeable stages were observed in the solution of the problem considered. These were namely the *early stage* and the *later stage*. The *early stage* usually lasts for a very short period of time during which sharp changes in the distribution of certain field variables, such as $\langle P_\gamma \rangle^\gamma$, $\langle \rho_\gamma \rangle^\gamma$, and $\langle u_\gamma \rangle$, occur due to the step change boundary conditions which cause very strong transient effects.

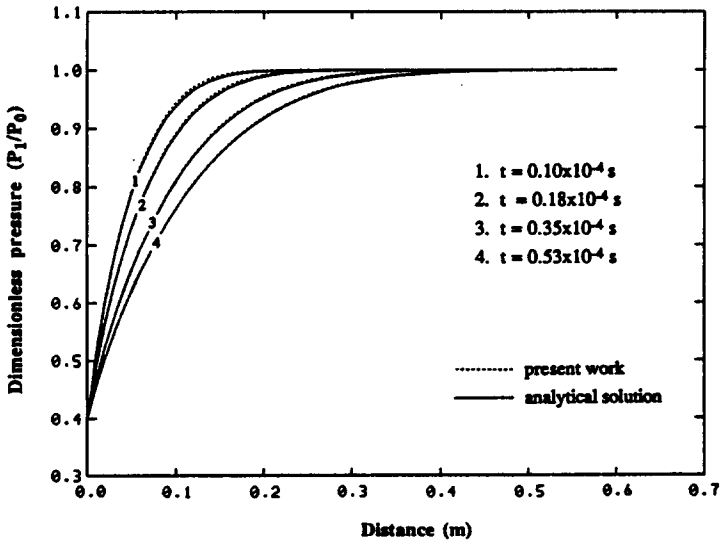

FIG. 3. Comparison of the numerical results with the analytical results in ref. [18].

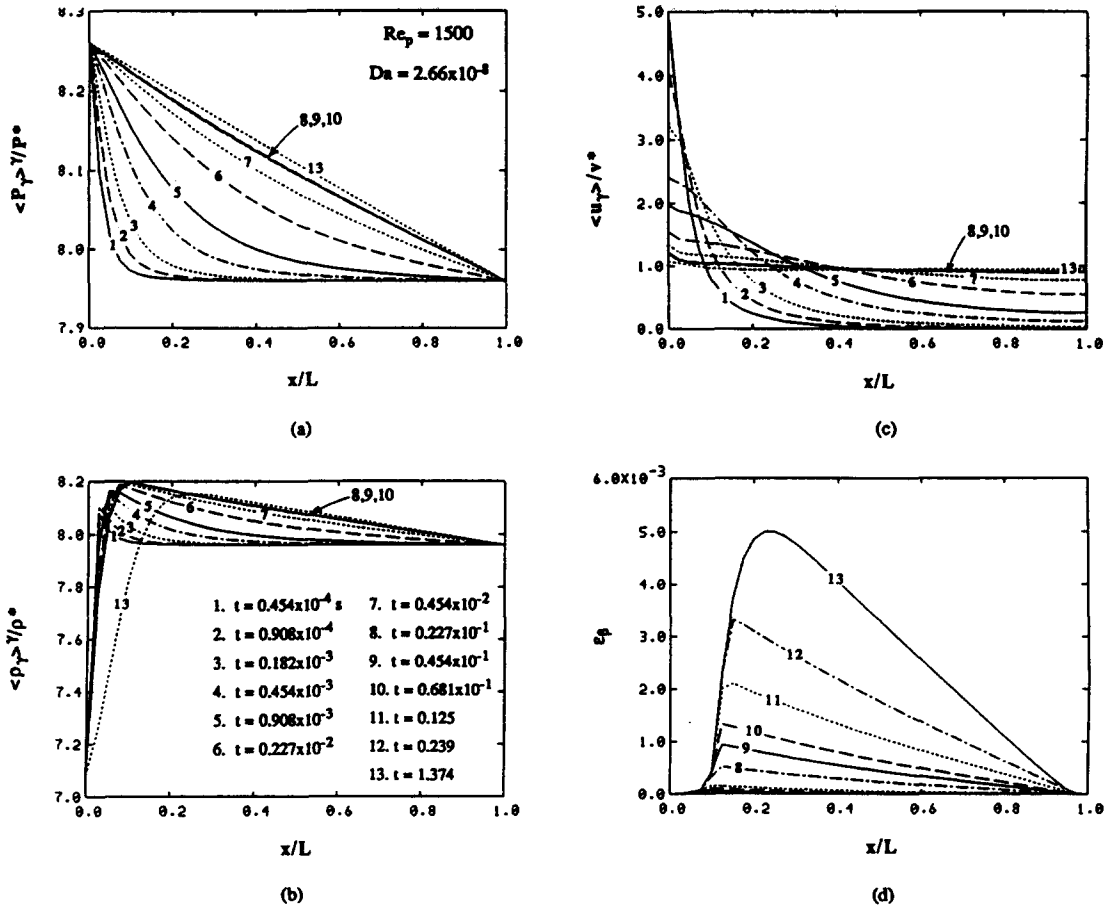

FIG. 4. Distribution of field variables during the *early stage*.

Solution of the problem with insulated wall boundary conditions. Figure 4 depicts the variations of the density, velocity and pressure of the vapor as well as the variation of the liquid fraction during the *early stage* at the mid-plane of the packed bed for insulated wall conditions for a case in which lead was used as the solid phase. It was found that, for cases with insulated boundary conditions, one-dimensional formulation would be very accurate since the variation of the main field variables in the y-direction did not exceed 1%. Figure 4(a) shows that the vapor pressure distribution evolves and becomes almost linear during the *early stage*. There is no appreciable thermal penetration during this period and the spatial variation of the vapor density follows the same trend as the vapor pressure as dictated by the equation of state. The temporal increase in the density is a result of the transient effects dictated by the vapor phase continuity equation. At points where vapor density reaches the saturation vapor density, condensation occurs and the liquid phase accumulates, thus yielding the variation of the liquid fraction as shown in Fig. 4(d). In Fig. 4 the *early stage* was extended to include the time during which more than 99% of the condensation took place for this case.

Beyond the *early stage*, the changes in the field variables are mainly caused by the development of the thermal penetration depth since the pressure distribution remains almost unchanged. Variation of the field variables of interest by time during the *later stage* are shown in Fig. 5. In Fig. 5(a) the solid lines depict the solid phase temperature distribution while the dotted lines depict the fluid phase temperature distribution. During the *early stage*, the effect of the transient term as well as the condensation (source) term in the vapor continuity equation dies away and, therefore, the vapor density variation in time during the *later stage* becomes dependent on the convective term in this equation. The mass flow rate in the packed bed becomes constant requiring an inverse relationship between the vapor density and velocity. Figures 5(c) and (d) clearly shows this behavior as a mirror image type of trend in the variations of the vapor density and vapor velocity at any instant. The spatial variation in the vapor density, on the other hand, can be explained from the equation of state. At any instant before the packed bed is fully charged, the slope of the vapor temperature profile will be larger than the slope of the vapor pressure profile for a certain length of the packed bed (meaning a sharper decrease in tem-

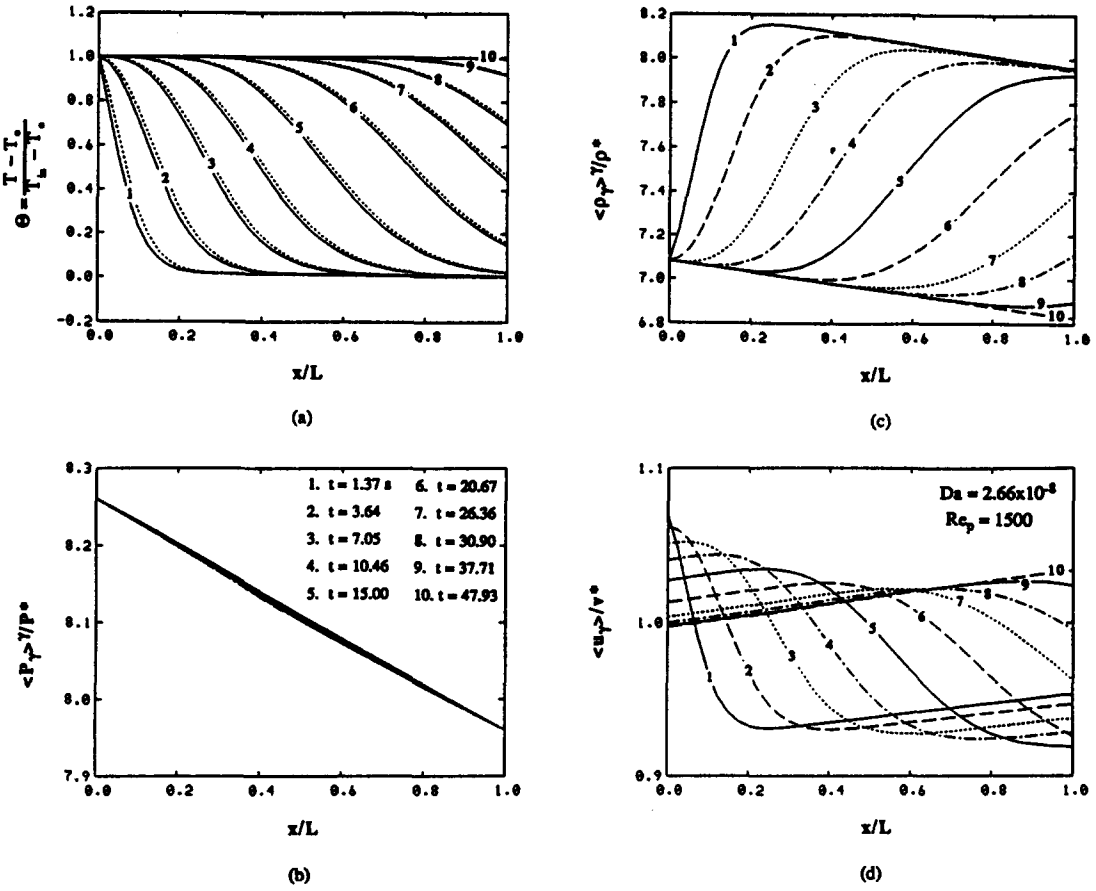

FIG. 5. Distribution of field variables during the *later stage*.

perature than in pressure) causing an increase in the vapor density, whereas exactly the opposite behavior can be seen at the locations where the slope of the vapor temperature profile is smaller than that of the vapor pressure profile (meaning a sharper decrease in pressure than in temperature). When the packed bed becomes thermally fully charged, the vapor density variation follows exactly the same trend as that of the vapor pressure as dictated by the equation of state.

The overall condensation rate in the packed bed was computed by integrating the individual condensation rates at all the grid points over the associated volumes at each time step. The average overall condensation rate per unit width of packed bed for the case for which the *early* and *later stage* results have been presented is depicted in Fig. 6(a). It can be seen that the overall condensation rate is higher at the beginning when the transient effects are very strong, and dies away as the sharp changes in the vapor density variation die away. The accumulative condensate in the packed bed was also computed by integrating the condensation rates at all grid points over the associated volumes at each time step and totaling with the previous sum. Figure 6(b) shows the variation in time of the amount of total condensate in the packed bed per unit width of the bed. As may be seen from this figure, the accumulation is fast at the beginning due to a high condensation rate, and builds up quickly reaching an asymptotic value in a short time.

The variation in the amount of thermal energy flowing into and out of the packed bed per unit width is depicted as a function of time in Fig. 7(a). These were computed by integrating the mass fluxes of the vapor flowing into and out of the packed bed over the inlet and the exit cross-sections. A very short section of the history of the thermal charging process at the beginning was left out in this figure in order to obtain a better scale that shows the variation of the heat flow rates clearly for the whole charging duration. Figure 7(b) shows the net energy stored per unit width of the packed bed as a function of time. The value of the total net energy stored in the packed bed was also determined by a thermodynamic balance analysis between the initial and the final (fully charged) states of the packed bed. The result of the numerical computation was found to be in very good agreement with this analytical result.

Solution of the problem with constant temperature wall boundary conditions. The same problem was solved for constant temperature top and bottom wall boundary conditions. As expected, strong two-dimensional behavior was found in the variations of many

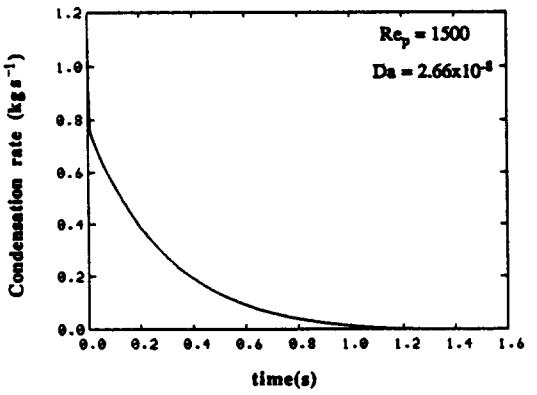

(a)

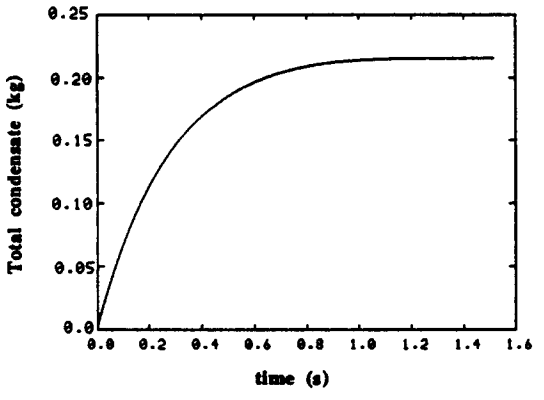

(b)

FIG. 6. (a) Variation of the average overall condensation rate in the packed bed per unit width. (b) Variation of the amount of total condensate in the packed bed per unit width.

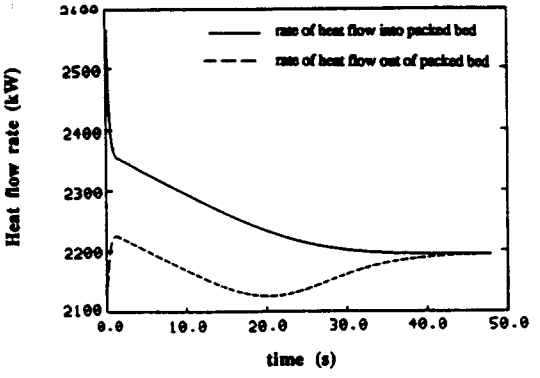

(a)

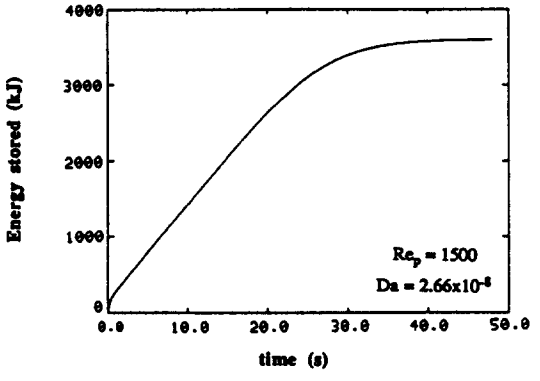

(b)

FIG. 7. (a) Rate of heat flow at the inlet and the exit of the packed bed per unit width. (b) Thermal charging of the packed bed.

of the field variables. Therefore, rather than presenting the results in the format of the previous section we will revert to two-dimensional contour plots for the field variable distributions. It should be noted that the solution of this problem has *early stage* and *later stage* parts just as in the case of insulated boundary conditions. For space economy, however, the distribution of three field variables at three time levels in the *later stage* will be presented here. These will be sufficient to show the two-dimensional behavior of the problem which becomes apparent during the *later stage*.

Figure 8 depicts the distributions of the fluid temperature, solid temperature and the vapor density in the packed bed at three different time levels. It can be seen from this figure that, although the two-dimensional behavior of the field variables is not very significant at the beginning, it becomes very much pronounced as the thermal penetration in the bed advances. In the core region of the packed bed the advancement of the temperature distribution follows a similar trend as in the case of insulated boundary conditions. Near the top and bottom walls, however, there is a temperature gradient in the y-direction due to heat loss. Since the variation in the vapor pressure in the y-direction is not significant, the vapor density variation in this direction is primarily determined by the fluid temperature variation. Hence, at locations closer to the top and bottom walls where the fluid temperature becomes lower the vapor density becomes higher. In the core region of the packed bed the variation of the vapor density in the x-direction depends on the slopes of the temperature and pressure distribution in this direction. At points where the slope of the temperature distribution is sharper than the slope of the pressure distribution the density will be decreasing and vice versa.

The average overall condensation rate per unit width of the packed bed was computed in the same manner described in the previous section. Figure 9(a) shows the variation of this quantity in time. Upon

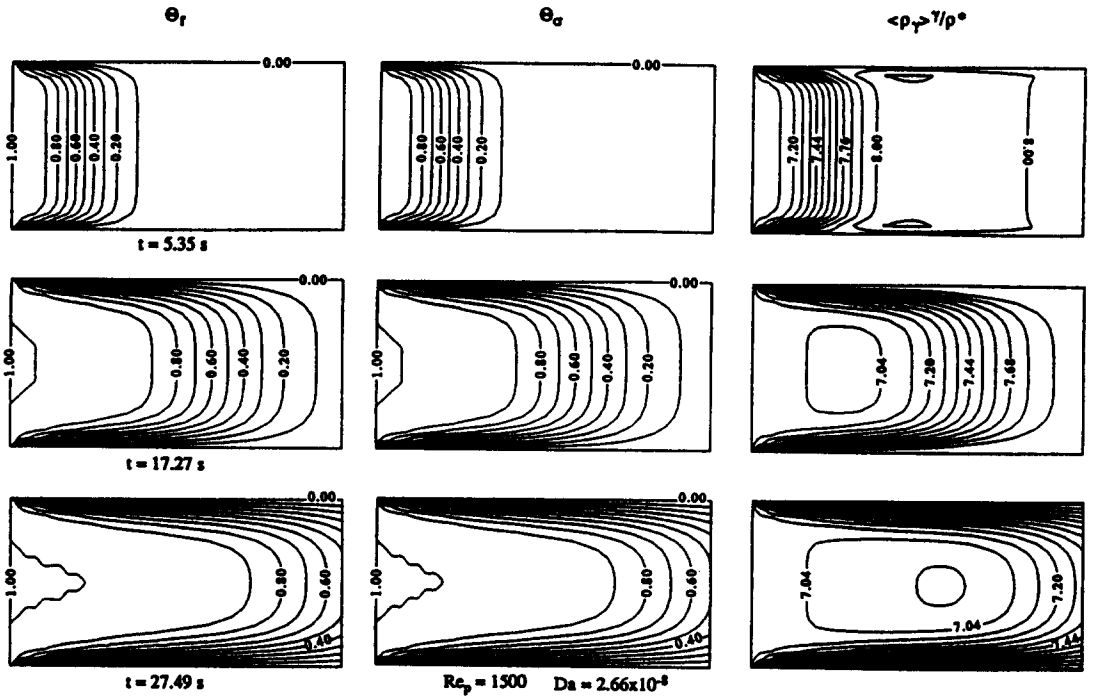

FIG. 8. Distribution of the field variables in the packed bed during the *later stage*.

comparing Fig. 9(a) with Fig. 6(a), one can see that condensation lasts slightly longer in the case of constant wall temperature. This is reasonable since due to heat loss from the top and bottom it takes longer for the vapor phase to reach a temperature at which the saturation vapor density exceeds the vapor density for the points next to the top and bottom boundaries near the inlet of the packed bed. Hence the condensation time at these points is prolonged. This also gives rise to a slightly larger amount of total condensate in the packed bed. One can see this by comparing Fig. 9(b) with Fig. 6(b).

The variation in the amounts of heat flowing into and out of the packed bed per unit width at the inlet and exit are shown in Fig. 10(a) as functions of time. In this case too, a small time slice at the beginning of the charging process is omitted from this figure in order to obtain a better scale. Figure 10(b) depicts the energy input into the packed bed, the energy that is lost from the top and bottom walls by conduction, and the net energy stored in the packed bed per unit width of the bed.

Effect of particle Reynolds number (Re_p) on condensation. The effect of Re_p on condensation was investigated by running three cases with different Re_p while the Darcy number (Da) was kept constant (by keeping the particle diameter fixed). The solid phase in all these cases was lead. Different Re_p values were obtained by applying different inlet pressure boundary conditions for each case. Figure 11(a) depicts the variation of the average overall condensation rate per unit width of the packed bed for the cases in which the nominal Re_p values were 500, 1000, and 1500, respectively. The corresponding variations of the total condensate in the packed bed per unit width as functions of time are shown in Fig. 11(b). From these figures it becomes apparent that the higher the Re_p the higher will be the condensation rate and the total condensate accumulation, whereas the higher the Re_p the shorter will be the duration of condensation. Higher Re_p indicates higher mass flow rates as well as higher pressure difference applied across the packed bed (larger compression forces on the vapor phase), thus higher condensation rate. On the other hand, higher Re_p, due to higher pressure gradient applied means potential for faster propagation of the pressure, density and temperature distributions in the vapor phase and thus shorter condensation time.

Effect of Darcy number (Da) on condensation. The effect of Darcy number on condensation was studied by considering three different Da values while Re_p was kept fixed at 1500. Different Da values were obtained by changing the particle size. Figure 12 shows the variations of the average overall condensation rate and the total condensate accumulation in the packed bed per unit width as a function of time for Da values of 1.49×10^{-8}, 2.66×10^{-8}, and 1.067×10^{-7}. The corresponding d_p values were 0.75, 1.0, and 2.0 mm, respectively. As d_p increases and hence Da increases, the specific surface area of the particles decreases. This causes slower heat transfer between the solid and fluid phases and a faster advancement of the thermal penetration depth of the fluid phase (faster attainment of lower densities than the saturation vapor density at

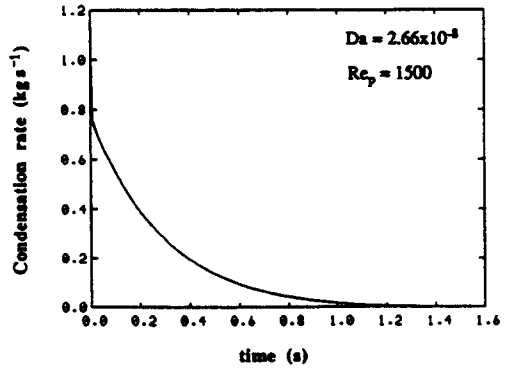

(a)

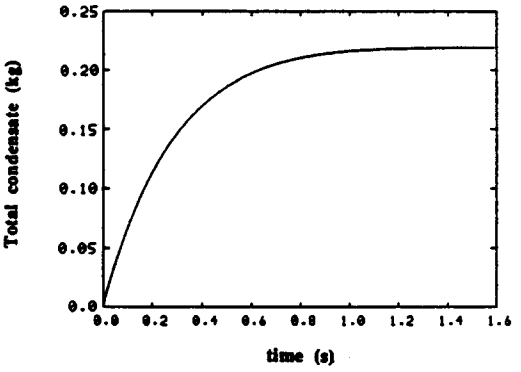

(b)

FIG. 9. (a) Variation of the average overall condensation rate in the packed bed per unit width. (b) Variation of the amount of total condensate in the packed bed per unit width.

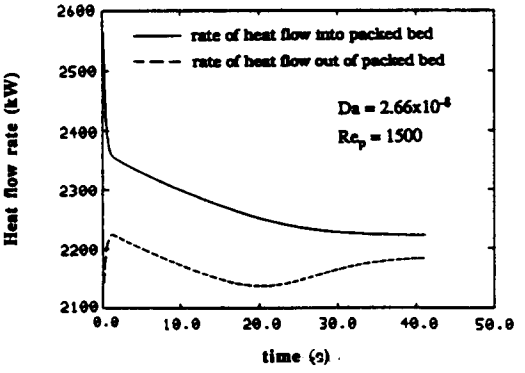

(a)

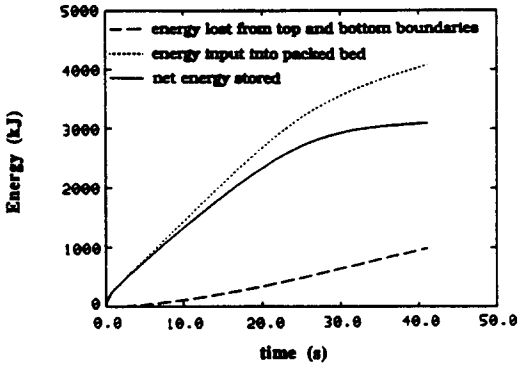

(b)

FIG. 10. (a) Rate of heat flow at the inlet and the exit of the packed bed per unit width. (b) Thermal charging of the packed bed.

the initial condensation points). Therefore, although the condensation zone advances faster the condensation rate and the amount of condensate accumulation remain small. Decreasing the d_p at constant Re_p (by increasing the pressure difference applied across the packed bed) increases the vapor velocities and hence larger mass flow rates and larger condensation rates. Also as d_p is reduced the specific surface area of the particles increases. The heat transfer between the solid and fluid phases becomes more vigorous and it takes longer for the fluid phase at the initial condensation points to reach temperatures high enough at which the vapor density becomes less than the saturation vapor density and condensation stops. Hence higher condensation rates are sustained for longer periods of time at these points, resulting in larger condensate accumulation.

Effect of thermal capacity of the solid phase on condensation. In order to analyze whether the thermal capacity of the solid phase utilized had any effect on condensation, a different material, namely 1% carbon steel, was employed as the solid phase material for qualitative comparisons. The variations of the average overall condensation rate and the total condensate accumulation per unit width of the packed bed as functions of time are depicted in Fig. 13 for the case of lead and steel as the solid material for three different Re_p values. As may be seen from this figure, although for a fixed Re_p the condensation rate is almost the same at the beginning for both solid materials, high condensation rates are sustained for a longer time in the case of steel than in the case of lead. The reason for this is that the thermal capacity of steel per unit volume is approximately 2.5 times that of lead. Due to this fact along with the high heat transfer rate between the solid and fluid phases, the temperature propagation in the solid and fluid phases will be slower in the case of steel than in the case of lead. In the case of steel the vapor phase will take a longer time to reach a high enough temperature at which the vapor density will become lower than the saturation vapor density corresponding to that temperature, and therefore, the condensation durations will be longer.

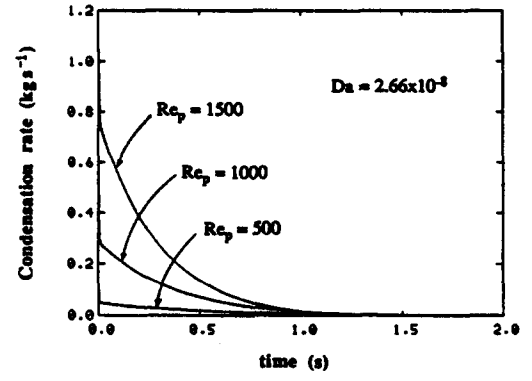

(a)

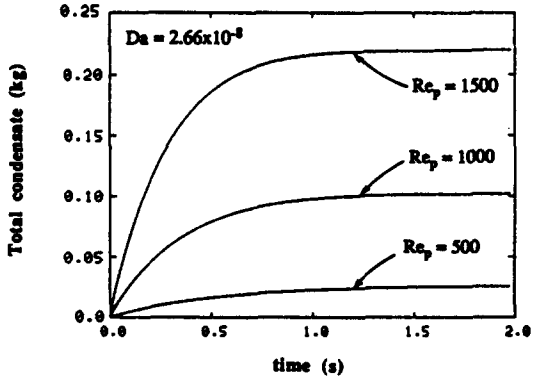

(b)

FIG. 11. Effect of particle Reynolds number on condensation.

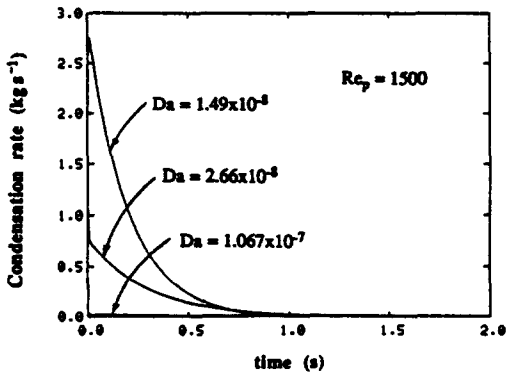

(a)

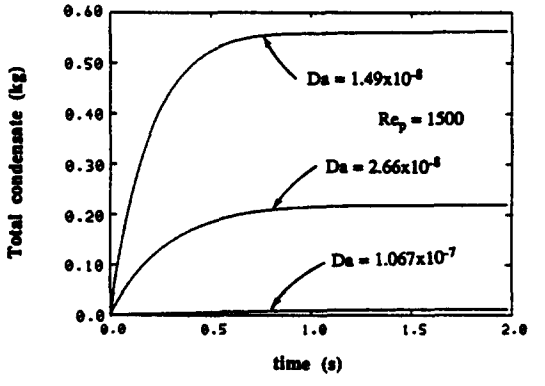

(b)

FIG. 12. Effect of Darcy number on condensation.

Effect of thermal capacity of the solid phase on the thermal charging of the packed bed. The thermal charging of the packed bed for two cases with different solid materials was investigated for insulated top and bottom boundary conditions. The two solid materials considered were lead and 1% carbon steel. The comparison of the thermal charging characteristics of these two cases is depicted in Fig. 14. As may be seen from this figure, although the charging behaviors are qualitatively similar in both cases, due to the larger thermal capacitance per unit volume of steel, it takes longer in the case of steel for the temperature of the working fluid at the exit of the packed bed to start rising. Therefore, there will be a high rate of energy stored in the packed bed for a longer duration of time in this case. Figure 14(b) shows that steel is a much better material than lead as an energy storage material since it has a lower density but yet higher thermal capacitance per unit volume compared to lead.

3.1. *General comments*

From the results obtained in the present study, it is possible to deduce useful information for physical applications. An interesting finding was the *early stage* of the problem. This stage was characterized by very strong transient effects. The very large velocities at the entrance of the packed bed suggest that this section should have a certain durability for withstanding the initial high compression forces due to the step change boundary condition in pressure. Also, during this stage, very rigorous heat interactions take place at the entrance region between the solid and the fluid phases.

This investigation showed that condensation in the working fluid is more drastic at the beginning due to the large compression forces which are present before the pressure distribution in the packed bed evolves into linear form. More condensate accumulates close to the entrance of the packed bed than close to the exit section. This qualitative behavior is important in applications in which it may become necessary at some point to remove condensate from the system in order to prevent the stalling of the packed bed due to large condensate accumulation. This study also showed that condensation can be controlled by different means. Namely, if continuous removal of heat from the packed bed can be maintained through the upper and lower walls, then the amount of condensation

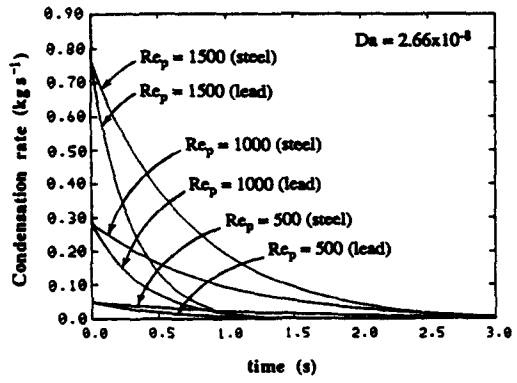

(a)

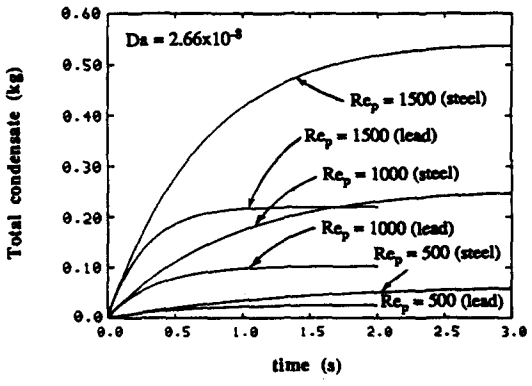

(b)

FIG. 13. Effect of the thermal capacity of the solid phase material on condensation.

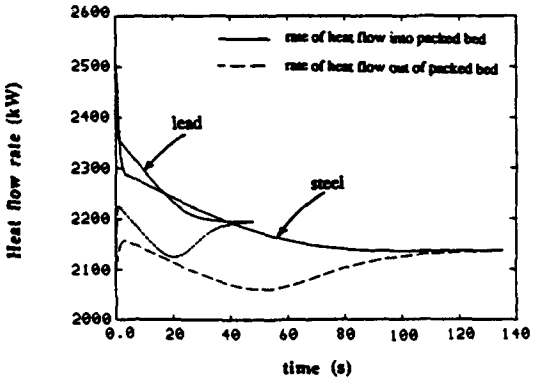

(a)

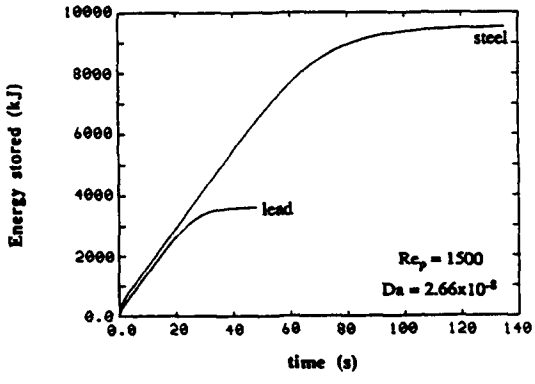

(b)

FIG. 14. (a) Rate of heat flow at the inlet and the exit of the packed bed per unit width. (b) Thermal charging of the packed bed.

can be increased. This can be achieved by the use of convective boundary conditions. Also, for a given size of the packed bed the amount of condensation for a set of specified boundary conditions can be controlled by the size of the particles chosen. Namely, by decreasing the particle size and hence increasing the heat interactions between the solid and fluid phases the amount of condensation can be increased and vice versa.

Also, initially the rate of energy storage in the packed bed was found to be high due to the large velocities of the working fluid. This fact makes this kind of energy storage system very suitable for applications in which there is pulsed heat to be stored. Results showed that once the vapor exit temperature starts rising the energy storage efficiency starts decreasing. Accordingly, the length of the packed bed can be chosen such that for the given energy storage requirement the thermal penetration front within the packed bed reaches close to the exit of the packed bed, and thus the thermal energy that escapes from being stored is minimized.

The study with constant wall temperature boundary conditions showed that the amount of heat which escapes from the packed bed by conduction in the transverse direction can be quite significant. This can be further enhanced by convective boundary conditions. A packed bed with insulated/convective boundary conditions can therefore be used as an energy storage/release unit in a closed loop system in applications in which waste heat comes in pulsed form and has to be removed during a certain consecutive period, such as in electronic waste heat removal systems and spacecraft thermal management systems.

4. CONCLUSIONS

From the results and discussions presented in the previous section, we can draw the following conclusions.

(1) For a fixed Da, larger Re_p values cause larger overall condensation rates and larger condensate accumulation.

(2) For a fixed Da, larger values of Re_p will result in smaller condensation durations.

(3) For a fixed Re_p, as Da is increased the overall condensation rate and the total condensate accumulation become smaller.

(4) As the heat capacity of the solid phase is increased, the overall condensation rate as well as the total condensate accumulation become larger.

(5) Constant wall temperature boundary conditions enhance the condensate accumulation in the packed bed as compared to insulated wall boundary conditions.

(6) Formulation without the local thermal equilibrium assumption is necessary for accurate computation of the condensation in the packed bed.

(7) Whereas one-dimensional formulation will give accurate results in the case of insulated boundary conditions, two-dimensional formulation is absolutely necessary for the case of constant wall temperature boundary conditions.

REFERENCES

1. K. Vafai and S. Whitaker, Simultaneous heat and mass transfer accompanied by phase change in porous insulation, *J. Heat Transfer* **108**, 132–140 (1986).
2. K. Vafai and S. Sarkar, Condensation effects in a fibrous insulation slab, *J. Heat Transfer* **108**, 667–675 (1986).
3. Y. Ogniewicz and C. L. Tien, Analysis of condensation in porous insulation, *Int. J. Heat Mass Transfer* **24**, 421–429 (1981).
4. K. S. Udell, Heat transfer in porous media considering phase change and capillarity—heat pipe effect, *Int. J. Heat Mass Transfer* **28**, 485–495 (1985).
5. E. R. G. Eckert and E. Pfender, Heat and mass transfer in porous media with phase change. In *Proc. 6th Int. Heat Transfer Conf.*, Vol. 6, pp. 1–12 (1980).
6. R. H. Nilson and P. C. Montoya, Experiments on transient condensing flow through a porous medium, *J. Heat Transfer* **102**, 489–494 (1980).
7. V. Ananthanarayanan, Y. Sahai, C. E. Mobley and R. A. Rapp, Modeling of fixed bed heat storage units utilizing phase change materials, *Metall. Trans. B* **18B**, 339–346 (1987).
8. K. Vafai and M. Sözen, Analysis of energy and momentum transport for a flow of a gas through a porous bed, *J. Heat Transfer* (1990), in press.
9. S. Whitaker, Simultaneous heat, mass, and momentum transfer in porous media: a theory of drying, *Adv. Heat Transfer* **13**, 119–203 (1977).
10. S. Ergun, Fluid flow through packed columns, *Chem. Engng Prog.* **48**, 89–94 (1952).
11. K. Vafai, Convective flow and heat transfer in variable-porosity media, *J. Fluid Mech.* **147**, 233–259 (1984).
12. K. S. Udell and J. S. Fitch, Heat and mass transfer in capillary porous media considering evaporation, condensation and non-condensable gas effects. In *Heat Transfer in Porous and Particulate Flows*, ASME HTD-Vol. 46, pp. 103–110 (1985).
13. M. Kaviany and M. Mittal, Funicular state in drying of a porous slab, *Int. J. Heat Mass Transfer* **30**, 1407–1418 (1987).
14. R. F. Benanati and C. B. Brosilow, Void fraction distribution in beds of spheres, *A.I.Ch.E. Jl* **8**(3), 359–361 (1962).
15. B. W. Gamson, G. Thodos and O. A. Hougen, Heat, mass and momentum transfer in the flow of gases through granular solids, *Trans. A.I.Ch.E.* **39**, 1–35 (1943).
16. F. A. L. Dullien, *Porous Media Fluid Transport and Pore Structure*, Chap. 3. Academic Press, New York (1979).
17. M. Riaz, Analytical solution for single- and two-phase models of packed-bed thermal storage systems, *J. Heat Transfer* **99**, 489–492 (1977).
18. R. E. Kidder and La Habra, Unsteady flow of a gas through a semi-infinite porous medium, *J. Appl. Mech.* **24**, 329–332 (1957).

ANALYSE DE L'ECOULEMENT AVEC CONDENSATION HORS D'EQUILIBRE THERMIQUE POUR UN GAZ TRAVERSANT UN LIT FIXE

Résumé—On analyse l'écoulement forcé avec condensation d'un gaz qui traverse un lit fixe. Le modèle développé n'utilise pas l'hypothèse d'équilibre thermique local entre le solide et les phases fluides. Les effets d'inertie et de viscosité sont considérés dans l'équation de quantité de mouvement de la vapeur en utilisant la relation d'Ergun–Forchheimer. On étudie le comportement thermique du lit fixe pour deux types différents de conditions aux limites et aussi la condensation dans la phase vapeur. Des comparaisons qualitatives des effets des différents paramètres sur la condensation révèlent que la différence de pression appliquée à travers le lit fixe, la taille des particules solides, et la capacité thermique de la phase liquide sont très influents sur la condensation. On observe que bien qu'un modèle bidimensionnel est essentiel pour des résultats précis dans le cas de conditions limites de température pariétale constante, un modèle monodimensionnel est satisfaisant dans le cas de conditions de frontières isolées thermiquement.

ANALYTISCHE UNTERSUCHUNG EINER KONDENSIERENDEN DAMPFSTRÖMUNG DURCH EIN FESTBETT

Zusammenfassung—In dieser Arbeit wird die instationäre erzwungene kondensierende Strömung eines Dampfes durch ein Festbett analysiert. Das entwickelte Modell enthält keine Annahmen über lokales thermisches Gleichgewicht zwischen Fest- und Flüssigphase. Sowohl Trägheits- als auch Zähigkeitskräfte wurden in der Impulsgleichung für die Dampfphase mit Hilfe der Ergun–Forchheimer-Beziehung berücksichtigt. Die thermische Beladung des Festbetts wird für Kondensation bei zwei verschiedenen Randbedingungen untersucht. Ein qualitativer Vergleich des Einflusses verschiedener Parameter auf die Kondensation zeigt, daß der Druckabfall im Festbett, die Teilchengröße der festen Phase und die Wärmekapazität der festen Phase starken Einfluß auf die Kondensation ausüben. Obwohl ein zweidimensionales Modell bei konstanter Wandtemperatur für genaue Ergebnisse notwendig ist, hätte bei idealer Isolierung der Wand auch ein eindimensionales Modell ausgereicht.

АНАЛИЗ ТЕЧЕНИЯ КОНДЕНСИРУЮЩЕГОСЯ ГАЗА ЧЕРЕЗ ПЛОТНЫЙ СЛОЙ ПРИ ОТСУТСТВИИ ТЕПЛОВОГО РАВНОВЕСИЯ

Аннотация—Анализируется неустановившееся вынужденное конвективное течение конденсирующегося газа через плотный слой. Разработанная для данного анализа модель не предполагает локального теплового равновесия между твердой и жидкой фазами. Инерционные и вязкостные эффекты описываются уравнением количества движения в паровой фазе с использованием соотношения Эргупа–Форшхаймера. Исследуются тепловая нагрузка плотного слоя при двух различных типах граничных условий и конденсация в паровой фазе. Качественное сравнение влияния различных параметров на процесе конденсации показало, что на него существенно влияют перепад давлений в плотном слое, размер частиц твердой фазы и ее теплоемкость. Выявлено, что, хотя двумерное моделирование давало точные результаты для случая граничных условий с постоянной температурой стенки, для случая граничных условий с изолированной стенкой вполне удовлетворительные результаты дает одномерное моделирование.